Carbohydrate Polymers 91 (2013) 305–313

Contents lists available at SciVerse ScienceDirect

Carbohydrate Polymers

journal homepage: www.elsevier.com/locate/carbpol

Glutaraldehyde–chitosan and poly (vinyl alcohol) blends, and fluorescence of their nano-silica composite films

Huawen Hu, John H. Xin, Hong Hu*, Allan Chan, Liang He

Institute of Textiles and Clothing, The Hong Kong Polytechnic University, Hong Kong

ARTICLE INFO

Article history:
Received 13 June 2012
Received in revised form 10 August 2012
Accepted 11 August 2012
Available online 19 August 2012

Keywords:
GA–chitosan
Poly (vinyl alcohol)
Nano-silica
Blend film
Nanocomposite film
Fluorescence

ABSTRACT

In this study, a commercial chitosan cross-linked with glutaraldehyde (GA–chitosan) having the autofluorescent property was effectively blended with a poly (vinyl alcohol) (PVA) matrix, in the formation of a transparent and fluorescent blend film. The fluorescent efficiency of the film was enhanced with red-shifted emission band by increasing the concentrations of the GA–chitosan and decreasing the PVA crystallinity. It was found that the incorporation of silica nanoparticles could further decrease the PVA crystallinity, enhance the fluorescent efficiency, and largely redshift the emission band, as compared with the neat GA–chitosan–PVA blend film. This fluorescent property could be finely tuned by careful doping of the silica nanoparticles and change of the PVA crystallinity. These phenomena could be reasonably explained by high extent of isolation of the fluorophores, increase of the stiffness of the fluorescent conjugated planar structure, and further decrease of the PVA crystallinity. In addition, the introduction of the nano-silica could improve the water and heat resistances of the GA–chitosan–PVA based silica nanocomposites.

1. Introduction

Isolated chitosan, a polysaccharide, is the linear and partly acetylated (1-4)-2-amino-2-deoxy-β-D-glucan (Muzzarelli, 1977; Ravi Kumar, Muzzarelli, Muzzarelli, Sashiwa, & Domb, 2004), which has polymorphism forms of anti-parallel fashion similar to that of α-chitin (Wang, Turhan, & Gunasekaran, 2004). Isolated chitosan is sensitive to acidic solution, and hydrophilicity is a very important characteristic for this material and it is, in part, due to the presence of the amine groups (Neto et al., 2005). Therefore, it is important to prevent it from readily dissolving in acid media and to enhance its chemical resistance, and at the same time, to maintain its hydrophilicity and long-term biological degradation. That can be realized by removing a certain amount of amine groups from it through the cross-linking reaction, but still preserving a part of free amine groups (Neto et al., 2005). Glutaraldehyde is a commonly used cross-linking agent. Recently, it has been found that the pristine chitosan cross-linked with glutaraldehyde (GA–chitosan) is autofluorescent, without the need of conjugating any external fluorochromes. By contrast, there is no fluorescent signal in the pure chitosan or glutaraldehyde emulsions (Wei et al., 2007). However, the neat autofluorescent GA–chitosan has some limitations such as brittleness and low air barrier properties. Blending the pure chitosan with poly (vinyl alcohol) (PVA) could be an effective way to improve its properties for practical applications.

Poly (vinyl alcohol) (PVA) is one of the widely used synthetic polymers owning to its excellent physical properties such as high tensile strength and flexibility, superior barrier to oxygen and aroma, and ease of formation in films. It is also biodegradable under suitable conditions. In addition, PVA is biocompatible and nontoxic. Because of these excellent properties, PVA films have been developed for biomedical applications.

Considering the usefulness of the chitosan and PVA in biological activities, a combination of these two polymers may have beneficial effects on the biological characteristics of the resulting composites. Besides, there is a huge amount of hydroxyl functional groups in the PVA molecular chains. The GA–chitosan also has abundant hydroxyl groups and preserved amine groups. These groups can lead to the formation of strong hydrogen bonds in the GA–chitosan–PVA blend system. As the PVA and GA–chitosan molecules can interpenetrate and intertwine with each other, the homogeneous blend can be formed. The specific inter-molecular interactions between the PVA and chitosan make the PVA/chitosan blend have good mechanical properties. The toughness and water resistance of the blends can be markedly enhanced as well as compared with the chitosan homopolymer and the pure PVA, respectively. Various applications of the PVA/chitosan blends has been widely reported, such as medical devices and controlled

* Corresponding author at: ST742, Institute of Textiles and Clothing, The Hong Kong Polytechnic University, Hung Hom, Hong Kong. Tel.: +852 3400 3089; fax: +852 2773 1432.
E-mail address: tchuhong@polyu.edu.hk (H. Hu).

0144-8617/$ – see front matter © 2012 Elsevier Ltd. All rights reserved.
http://dx.doi.org/10.1016/j.carbpol.2012.08.038

delivery of drugs (Chandy & Sharma, 1992; Chuang, Young, Yao, & Chiu, 1999; Koyano, Koshizaki, Umehara, Nagura, & Minoura, 2000; Minoura et al., 1998; Nakatsuka & Andrady, 1992; Srinivasa, Ramesh, Kumar, & Tharanathan, 2003; Yang, Su, Leu, & Yang, 2004; Yu, Song, Shi, Xu, & Bin, 2011).

In this study, the chitosan partially cross-linked with glutaraldehyde was blended with a PVA matrix to form a transparent blend film having fluorescent property. The partial cross-linking reaction between the amine groups of chitosan and the aldehyde groups of glutaraldehyde leads to the formation of the autofluorescent chitosan with the residual amine groups in it. Due to the abundant hydroxyl and preserved amine groups, the GA–chitosan can be dissolved into hot acidic water solution, and easily compounded with PVA matrix, without the sacrifice of the autofluorescent properties.

Recently, a wide range of nano-materials has been designed and used in different areas, such as medicine, cosmetics, and foods (Hiromi et al., 2011). Among them, it is necessary to note that the nano-silica has been widely explored for various applications, such as fluorophore carrier (Ow et al., 2005), controlled release of drug molecules, antiseptic agents (Depla et al., 2011; Verraedt, Pendela, Adams, Hoogmartens, & Martens, 2010), and biosensor, etc. (Monton, Forsberg, & Brennan, 2012). It is well known that there exist plenty of the silanol groups in the nano-silica, which can increase hydrogen bonding effects in a composite system, change the crystalline behaviors of polymeric blended matrix, and affect the fluorescent properties of end products. On the other hand, thermal resistance is one of the most dominative properties for polymeric materials, as it ultimately governs the mechanical properties, durability, spectral stability, shelf lives, and life cycles of polymers (Cho, Jung, Cho, Lee, & Shim, 2003; Jin et al., 2003; Peng & Kong, 2007; Peng, Kong, Li, & Spiridonov, 2006; Xia et al., 2005). Once the degradation begins, the above properties will gradually deteriorate. Hence, the incorporation of inorganic nano-silica with the GA–chitosan–PVA blend matrix was also considered in this study to change the fluorescent property, and to improve the thermal resistance of the GA–chitosan–PVA blend. Due to the large amount of the silanol groups, the nano-silica can be well dispersed within the PVA matrix, facilitating the manufacturing of fluorescent nanocomposites. It is expected that the fluorescent PVA based blend and its silica nanocomposites developed in the present work could pave a way for the fluorescent probe, drug-carrier, and tracer applications.

2. Materials and methods

2.1. Materials

PVA powder (99% hydrolyzed) of a typical Mw 89,000–98,000 was supplied by Sigma–Aldrich Chemical Co. Inc. The GA–chitosan powder, with ~18% amine groups in its polymeric chains cross-linked with glutaraldehyde and ~70% free amine groups left behind, was kindly supplied by Sunshine Road Biomaterials Technology Co. Ltd. (Shenzhen, China). Silicon dioxide nanopowder with an average diameter of 5–15 nm (BET) was purchased from Sigma–Aldrich Chemical Co. Inc. Acetic acid (100%, A.R. grade) was obtained from Oriental Chemicals and Lab. Supplies Ltd., Hong Kong. All chemicals were directly used without further purification.

2.2. Preparation of GA–chitosan–PVA blend and its nanocomposite film with silica nanoparticles

A certain amount of GA–chitosan powder was dissolved in 100 mL of dilute acetic acid (2%, w/w) at 70 °C in a beaker placed in a thermostatic oil bath equipped with a mechanical stirring device (the reaction lasted for about 1 h until no insolubles were visible). PVA pellets were dissolved in deionized water at about 85 °C for 1 h. Then, GA–chitosan and PVA solutions were compounded together by mechanical stirring at 75 °C for 2 h, followed by another 1 h of stirring under room temperature to obtain a homogeneous blend. The clear solution was then cast on a glass plate, and gradually dried at 60 °C for 48 h. To neutralize the acetic acid contained in the composite film, the latter was immersed in a 4% NaOH aqueous solution for 1 h, then thoroughly washed with deionized water, and finally dried at 60 °C for 48 h. Pure PVA and PVA based blend films with various concentrations of GA–chitosan were prepared with the same procedure.

A given amount of nano-silica powder was dispersed into deionized water with the assistance of mechanical stir and ultrasonic wave for about 2 h, and then a homogenous aqueous dispersion of nano-silica was obtained, followed by compounding GA–chitosan solution and nano-silica dispersion. The resultant clear dispersion was cast into a flat Petri dish and allowed to stand for about 2 h until no bubbles were observed. Finally, it was oven-dried at 60 °C for 48 h. A series of 8% GA–chitosan–PVA blend based nanocomposites with different loadings of silica nanoparticles were fabricated with the same procedure. As for the prepared samples, all percentages presented in this paper are the percentages of the weight of GA–chitosan or nano-silica related to the total weight of the composite.

2.3. Characterization

The structures of the powder and film samples were analyzed using a Fourier transformed infrared spectrometer (FTIR, Perkin Elmer System 2000). The FTIR spectra of the powder samples were recorded using KBr pellet technique, and the PVA based film samples were tested in the mode of attenuated total reflection (ATR). The UV–vis spectra of the composite film samples were measured with a UV–vis spectrometer (Lambda 2S, Perkin Elmer), and their fluorescence spectra were recorded with a Perkin-Elmer Luminescence spectrometer LS50B, which was equipped with a motor-driven linear polarizer on the detection side, at room temperature under isotropic excitation. The crystalline and glass transition behaviors of the pure PVA and its composites filled with the GA–chitosan and nano-silica were measured by a differential scanning calorimeter (DSC, Perkin Elmer DSC-7) according to the following way: 10 mg of sample was firstly sealed in an Al pans, heated from 25 to 250 °C with a rate of 10 °C/min, kept at 250 °C for 3 min, then cooled from 250 to 25 °C with a rate of −10 °C/min and kept at 25 °C for 3 min, and finally heated again from 25 to 250 °C with a rate of 10 °C/min. The cooling and second heating stages were selected for the analysis. Thermogravimetric analysis (TGA) of the samples was carried out on a Mettler Toledo TGA/SDTA851 under N_2 atmosphere with a heating rate of 10 °C/min. The morphologies of pristine GA–chitosan and nano-silica powders, and freeze-fractured sections of PVA based composites were investigated using a field-emission scanning electron microscopy (FE-SEM, JEOL JSM-6335F). Before SEM observation, all the samples were coated with a thin layer of platinum. The crystallinity of the pure PVA and its composite materials were studied by a X-ray diffraction device equipped with 9000 W Cu Kα X-Ray tubes (XRD, Bruker D8 Advance X-ray diffractometer, Bruker AXS, Karlsruhe, Germany) operating at 45 kV and 200 mA.

3. Results and discussion

It is well known that the generation of fluorescence results from π–π^* and n–π^* transitions of the unsaturated bonds, and that the fluorescence of a material has a close relationship with the following special structure features: (1) the structure with large

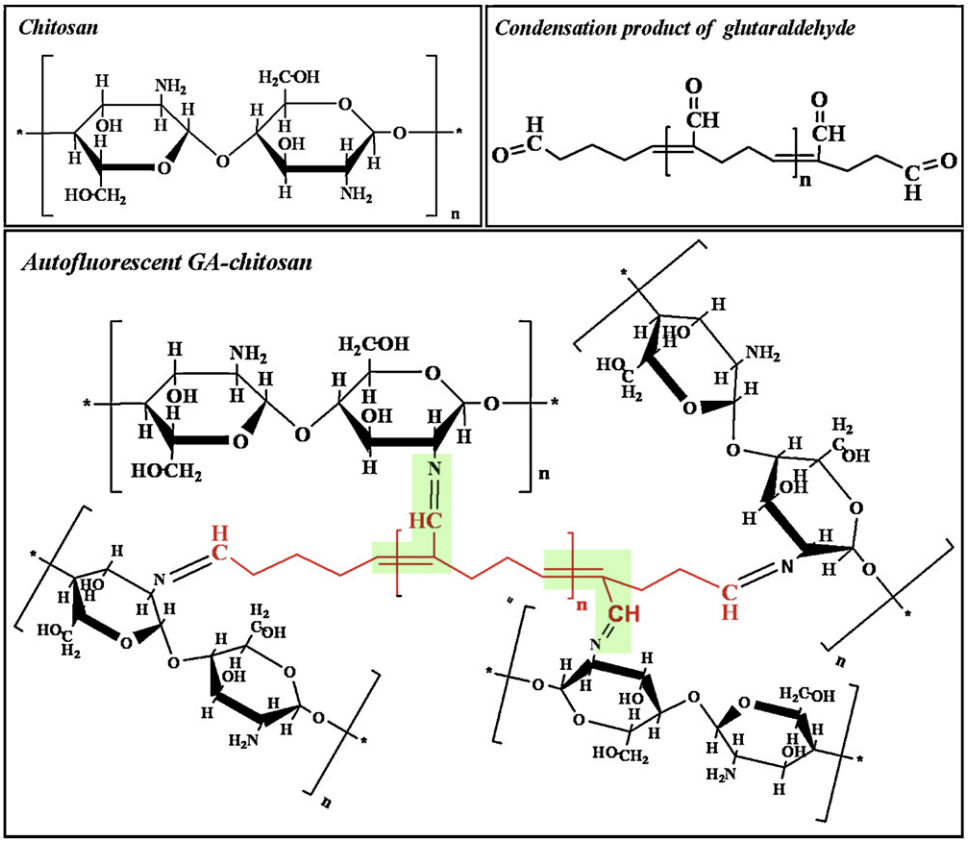

Fig. 1. Schematic presentations of the formulae of chitosan, condensation product of glutaraldehyde, and GA–chitosan.

conjugated π bonding; (2) stiff planar structure; (3) electron-donor substituents that can enhance the fluorescent effect, and electron-acceptor substituents that can attenuate the fluorescent effect; (4) the structure feature of the lowest excited singlet state (the S1 state): the π–π^* transition generates a stronger fluorescence, while the n–π^* transition a weaker fluorescence.

Chitosan exhibits an intriguing property when it is chemically cross-linked with glutaraldehyde. The cross-linked chitosan displays autofluorescent properties without the need to conjugate any external fluorochromes (Wei et al., 2007). The autofluorescent mechanism is illustrated in Fig. 1. As reported by Goldsmith and Brezina (1982), glutaraldehyde will be condensed and dehydrated into unsaturated α–β double bonds (—C═C—) in the form of condensation product. According to the reaction formula of chitosan and condensation product of glutaraldehyde, two different kinds of double bonds can be found in the structure of GA–chitosan, i.e., —C═C— from condensation moiety of glutaraldehyde, and —C═N— from the cross-linking reaction moiety between the amine groups in chitosan and aldehyde groups in the condensation product of glutaraldehyde. The two kinds of double bonds form a conjugated planar structure in the GA–chitosan, enabling the GA–chitosan to be autofluorescent, as specially marked in Fig. 1.

FTIR spectra are a useful tool to identify the presence of certain functional groups in a molecule as each specific chemical bond often has a unique energy absorption band. FTIR spectra obtained for GA–chitosan, pure PVA, and PVA based blend and nanocomposite materials are presented in Fig. 2. For GA–chitosan, two typical absorption peaks can be observed. The peak with a strong intensity centered at 1658 cm^{-1} is attributed to the imine bond (C═N) and the peak at 1595 cm^{-1} is associated with the C═C bond. The results confirm that there are two kinds of unsaturated double bonds in the GA–chitosan. The similar FTIR results of a glutaraldehyde cross-linked chitosan microspheres were also reported by Wei et al. (2007). In addition, the preserved amine groups in GA–chitosan can be reflected by the double absorption peaks, centered at about 3300 and 3367 cm^{-1}, as marked by two parallel dotted lines. With respect to the pure PVA, the absorption bands can be observed at 3280 (OH stretching vibration from intra-/inter-molecular hydrogen bonded hydroxyl groups), 2850–3000 (alkyl stretching), 1436 (C—H bending), 1335 (O—H bending), 1245 (residual acetate), 1100 (C═O deformation), and 929 cm^{-1} (out-of-plane deformations of intra-/inter-molecular hydrogen bonded OH

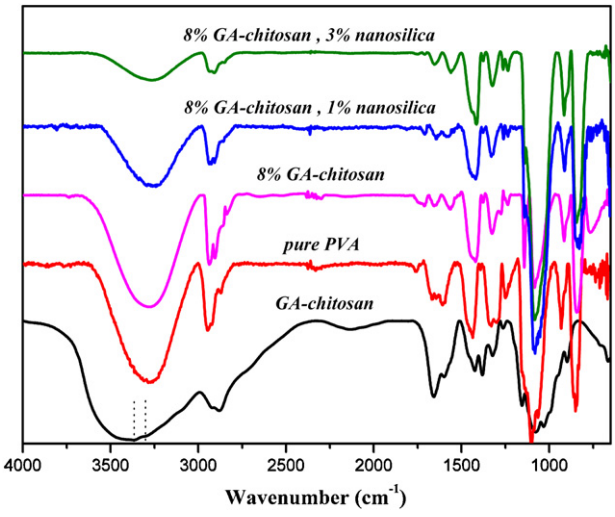

Fig. 2. FTIR spectra of the GA–chitosan, pure PVA, and PVA based blend and nanocomposite materials.

groups) (Bruni et al., 2011; Yang, Lu, & Lickfield, 2002). Moreover, the band at 929 cm^{-1} derived from O—H out-of-plane deformations left shifts to 913 cm^{-1} with the incorporation of GA–chitosan and nano-silica. This shift to lower wave number (lower energy) reveals that the inter-molecular hydrogen bonding in PVA is attenuated (Ohno, Shimoaka, Akai, & Katsumoto, 2008; Yoon, Lee, & Stafford, 2011), which may be due to that the incorporated inclusions strongly interact with PVA molecules, and then disturb the interactions among PVA molecules. The strong interactions between PVA and GA–chitosan molecules can effectively isolate the GA–chitosan fluorophores, and enhance the fluorescent efficiency. In addition, the introduction of nano-silica makes the intensity of the band at 1100 cm^{-1} dramatically enhanced, which may be attributed to overlapping effect, from the introduction of a large amount of Si—O bonds, whose characteristic vibration signal is also located at 1100 cm^{-1}.

The XRD patterns of GA–chitosan and nano-silica are shown in Fig. 3(A). GA–chitosan presents two typical diffraction peaks, centered at about 20.2 and 10.7°, respectively. It should be noted that the maximum intensity of the characteristic diffraction peak of GA–chitosan is about 600, which is much lower than that of the native chitosan (as high as 13,000) reported by Qi, Xu, Jiang, Hu, and Zou (2004) Moreover, the diffraction peaks of GA–chitosan are more broadened. These imply that the chain alignment of chitosan turns to be more disordered after the cross-linking reaction with glutaraldehyde. In addition, as for nanosilica, only a broad and weak absorption peak located at about 23.3° can be observed, indicating that the employed silica nanoparticles are in the form of an amorphous structure, rather than a crystalline structure (Chen et al., 2010; Jongsomjit, Chaichana, & Praserthdam, 2005).

Fig. 3(B) shows the XRD patterns of the GA–chitosan–PVA blends and its nanocomposites with nano-silica. It can be clearly observed that the diffraction intensity of the main crystalline plane of PVA is gradually decreased, which corresponds to the decrease of the crystallinity, after the introduction of GA–chitosan and SiO_2 nanoparticles. The PVA and GA–chitosan molecules interpenetrate and intertwine with each other, heavily disturbing the arrangement regularity among PVA or GA–chitosan molecules, and thus decreasing the crystallinity of both PVA and GA–chitosan. Similarly, the incorporation of nano-silica further increases the extent of chaos status of PVA and GA–chitosan molecules, leading to the further decrease of crystallinity. Selecting the pure PVA as a benchmark, the relative crystallinity can be calculated as the value of the main crystal plane diffraction area firstly divided by the peak area corresponding to the amorphous section, and then normalized by the ratio of the total diffraction peak area of the composite sample to the pure PVA sample. The relative crystallinity of different samples is shown in Fig. 3(C). When 4% GA–chitosan is firstly blended with PVA (sample (b)) matrix, the crystallinity of the blend is markedly decreased. If the concentration of GA–chitosan is further increased from 4% to 8%, the crystallinity continues to decrease, but the decreasing extent is lower that of the PVA blended with 4% GA–chitosan. When using the 8% GA–chitosan filled PVA blends as a matrix, the incorporation of different amounts of nano-silica will again reduce the crystallinity of the nanocomposites (from sample (e) to sample (h)). Although the crystallinity decreases with increasing the percentage of the nano-silica, the decreasing extent is reduced.

For further analysis of the crystallization behavior of different samples, DSC was employed to analyze the changes of the fusion and cold crystallization enthalpies. As clearly observed in Fig. 4(a) and (c), both enthalpies display a regular function relationship with inclusion type and content within PVA matrix. As shown in Fig. 4(a), in the heating process, the value of the crystal melting peak area decreases with first increase of the concentration of GA–chitosan from 4% to 8%, and then incorporation of nano-silica from 1% to

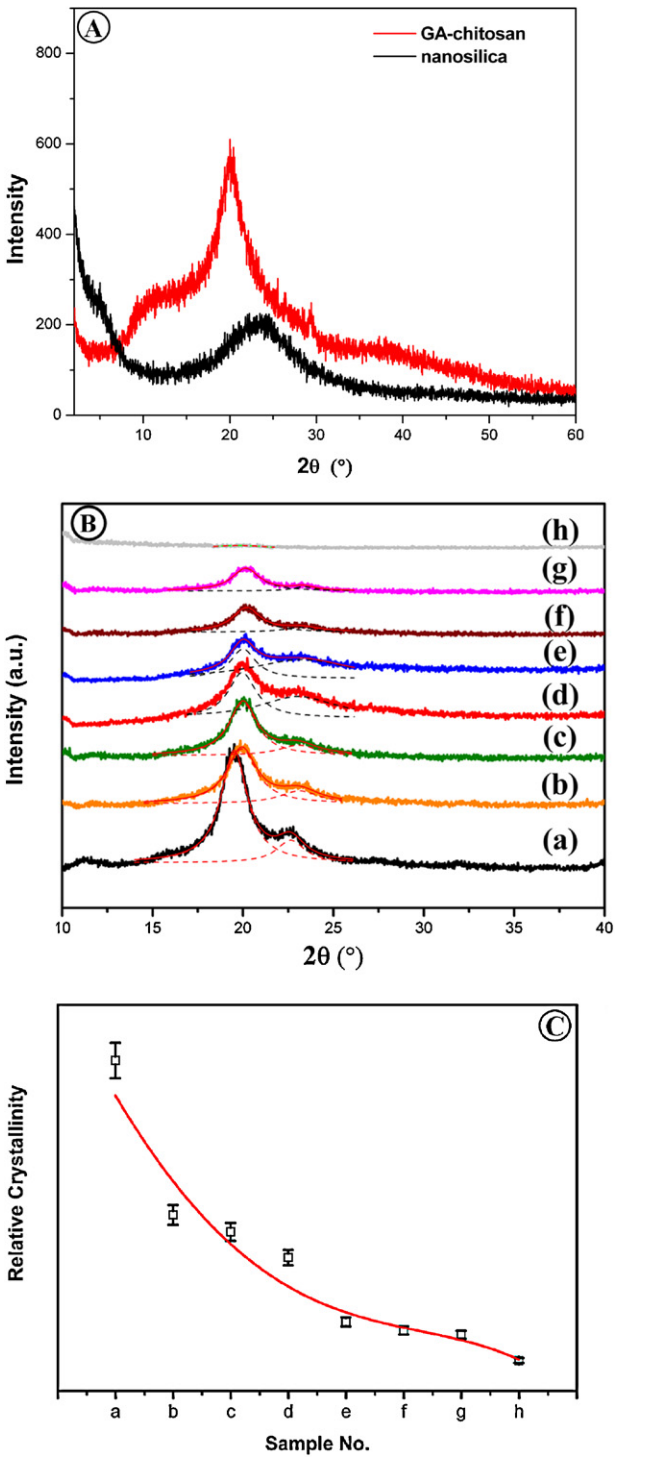

Fig. 3. (A) XRD patterns of the GA–chitosan and nano-silica; (B) XRD patterns of the pure PVA (a) and its blend films with 4% GA–chitosan (b), 6% GA–chitosan (c), and 8% GA–chitosan (d), and 8% GA–chitosan filled PVA blend based nanocomposite films with 1% (e), 3% (f), 5% (g), and 7% (h) nano-silica; (C) relative crystallinity of the pure PVA and its bend and nanocomposite materials deduced from the corresponding XRD patterns.

7%, along with increased melting range and left shift of the melting point. This indicates that the regularity degree of the molecular chain of the composite samples is largely reduced as compared with that of the pure PVA, resulting in a decrease of crystallinity. This also reflects that there exist dramatically strong molecular interactions between the inclusions and PVA matrix. The decrease of

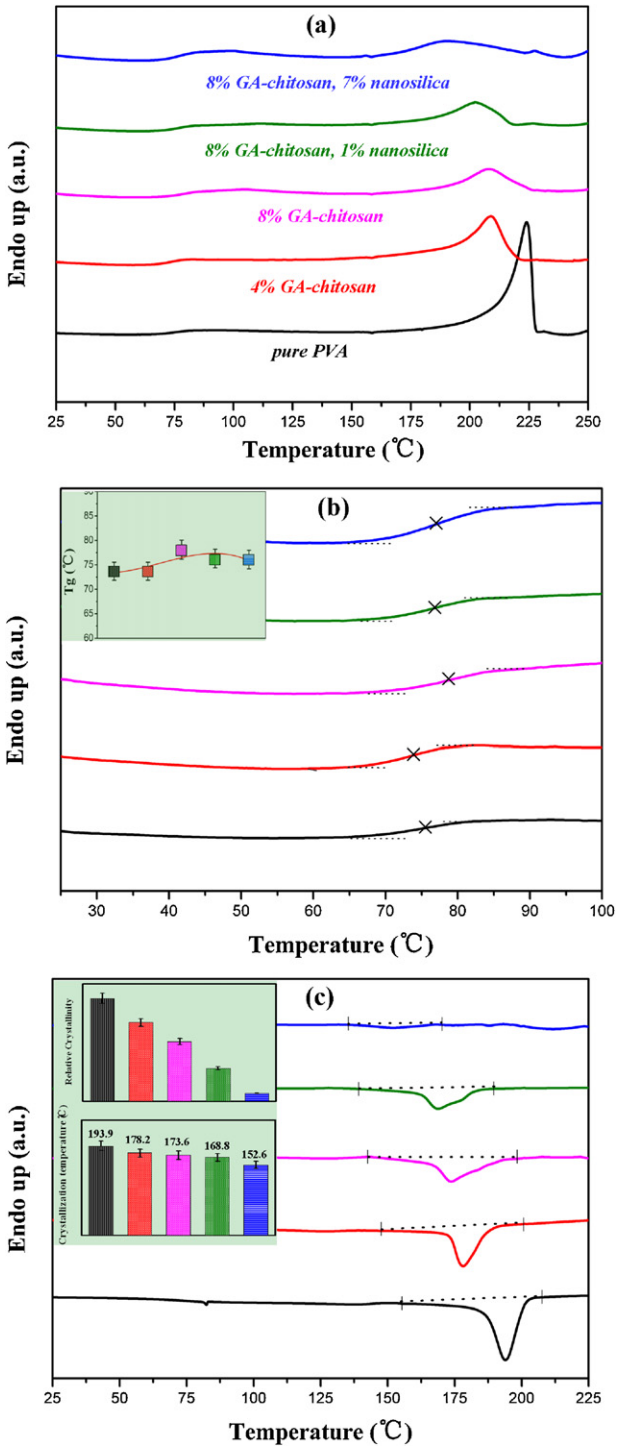

Fig. 4. DSC heating (a and b) and cooing (c) curves of the pure PVA and its blend and nanocomposite materials.

the crystallinity endows GA–chitosan with a molecular dispersion, and thus enables GA–chitosan to be highly effective in fluorescence. Likewise, in the cooling process, the crystallization enthalpy is decreased, together with the increased value of full width at half maximum (FWHM) and decreased crystallization temperature. The relative crystallinity is obtained by the integration of the peak area and following normalization by initial weight of the sample. The inserted graph in Fig. 4(c) illustrates the plots of relative crystallinity and crystallization point versus the type and content of inclusions. It can be seen that the value of relative crystallinity linearly decreases with increasing the GA–chitosan concentration and nano-silica content. The crystallization point linearly decreases as well but with a much smaller slope. The crystal melting process of the samples in the heating process is in good accordance with the reverse crystallization behaviors. As shown in Fig. 4(b), the glass transition behaviors are observed by extracting the low temperature range from DSC heating curve. It has been seen that the glass transition temperature (T_g), which reflects the relaxation dynamics of the polymer chain segments, is especially sensitive to the polymer molecule structure within composite materials (Bandi & Schiraldi, 2006). The T_g of the PVA matrix is unchanged after initially compounded with 4% GA–chitosan. There are two competing aspects affecting the glass transition behavior: (1) the reduction of crystallinity will decrease the value of T_g due to the lower extent of the confinement of molecular chain segments; (2) the interpenetration and entanglement of the GA–chitosan with PVA molecules, and the strong interactions such as inter-molecular hydrogen bonding, will lead to the retardant of the movement of the molecular chain sections, and thus result in the increase of the T_g value. The two competing aspects will counteract each other, and 4% GA–chitosan just has a balanced result. With increasing the GA–chitosan addition to 8%, the T_g shifts to a higher value, suggesting that the second aspect plays a main role in this competition. Based on the 8% GA–chitosan filled PVA blend (as a matrix), the incorporation of 1 and 5% nano-silica will decrease the T_g value. But the T_g values of the silica nanocomposites are higher than that of the pure PVA. Similarly, the aforementioned mechanism gives a reasonable explanation of the results. In addition, the silanol groups Si—OH in nano-silica will have an interaction with the functional groups in GA–chitosan, and thus may relieve the interactions between the molecules of GA–chitosan and PVA to a certain extent, leading to the decrease of T_g value, as compared with that of the 8% GA–chitosan–PVA blend.

The digital photographs displaying the transparence and fluorescence of our prepared samples are shown in Fig. 5. The words shaded by the 8% GA–chitosan filled PVA blend and its nanocomposite with 3% nano-silica can be clearly seen, which means that the excellent transparence is obtained, as shown in Fig. 5(a). If the incorporations of the GA–chitosan and nano-silica into the PVA matrix increase the crystallinity of PVA, the transparence will be generally decreased, due to the larger extent of light scattering and refraction. Therefore, the excellent transparence of the PVA based composite products may be partly due to the decrease of the crystallinity of PVA after the introduction of the GA–chitosan and nano-silica. This is in good agreement with DSC and XRD results. As shown in Fig. 5(b), under UV excitation, the composite films display strong fluorescence. With increasing the GA–chitosan concentration from 4% to 8%, the fluorescence intensity is increased owning to the enlarged conjugated system. In addition, the pure blue emission gradually turns to be aquamarine blue, attributable to the generation of new emission band red-shifted with respect to the main emission band, which can be confirmed by the fluorescence characterization. For the GA–chitosan–PVA blend based silica nanocomposites, the aquamarine blue phase shifts to be mild red, with increasing the nano-silica loadings. This indicates that the introduced nano-silica increases UV absorption and enhances the fluorescent efficiency. The strong interactions such as hydrogen bonding between the GA–chitosan and nano-silica increase the stiffness of the GA–chitosan conjugated structure, leading to the enhancement of the fluorescence. In addition, the decrease of crystallinity of GA–chitosan molecules means that the molecule alignment turns to be more disordered, and hence the molecule aggregation gets relieved, leading to the molecular dispersion of fluorophores and highly efficient fluorescence.

Fig. 6 shows the UV–vis absorption and fluorescent emission spectra of the GA–chitosan–PVA blend films and 8%

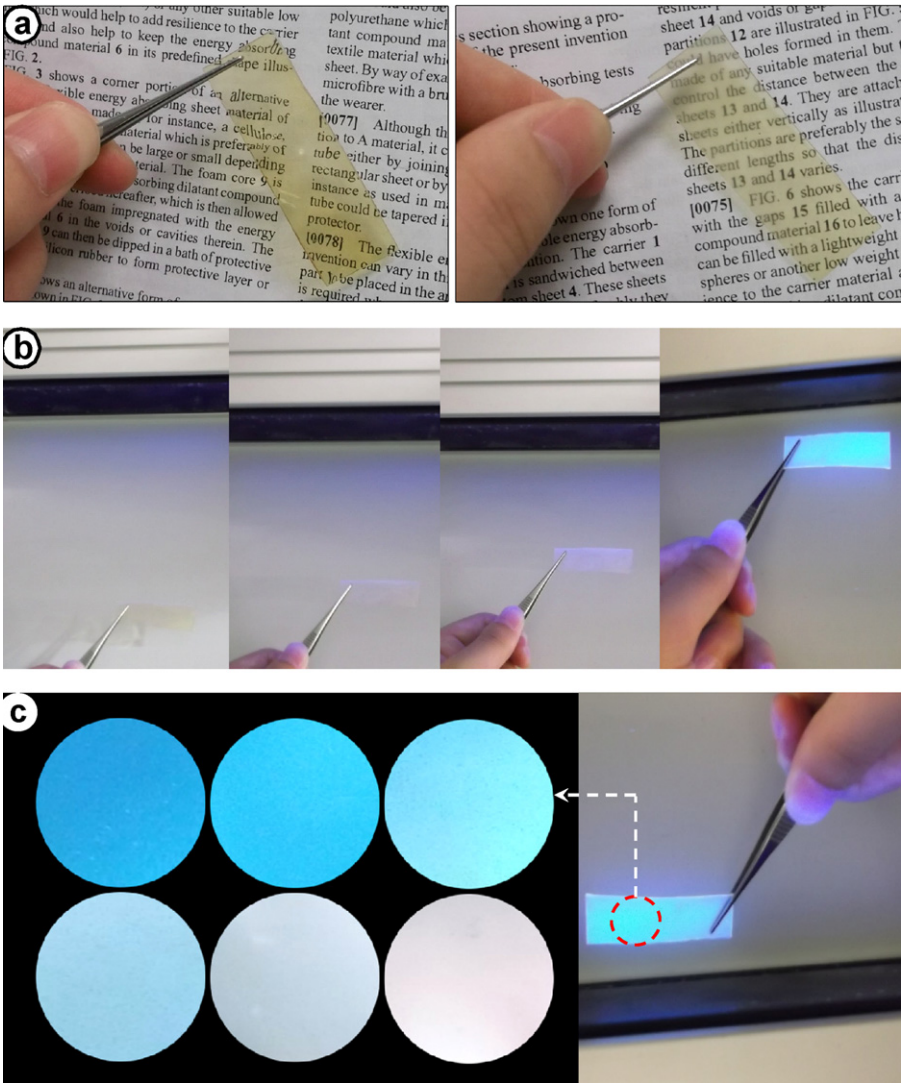

Fig. 5. (a) Digital images (under visible light) of the 8% GA–chitosan–PVA blend film (left one) and 8% GA–chitosan–PVA blend based nanocomposite film loaded with 3% nano-silica; (b) digital images showing the process of approaching a long-range UV lamp (λ = 365 nm) for the 8% GA–chitosan–PVA blend film; (c) digital images (under excitation with a long-range UV lamp (λ = 365 nm)) of the PVA/GA–chitosan blends with GA–chitosan concentrations of 4%, 6%, and 8% (upper layer from left to right), and 8% GA–chitosan–PVA blend based nanocomposites with nano-silica loadings of 1%, 3% and 5% (bottom layer from left to right).

GA–chitosan–PVA blend based nanocomposite films with the inclusion of silica nanoparticles. The UV–vis spectra of the PVA/GA–chitosan blend films show broad absorption bands centered at about 280 nm (mostly located in the middle-UV region of the electromagnetic spectrum of the light), along with the increase of the intensity with increasing the GA–chitosan concentration (Fig. 6(a)). In particular, despite the high scattering contribution of the 0.5 mm thick PVA matrix, the films do not display any absorption band attributed to the formation of GA–chitosan aggregates. However, different from the UV–vis absorption spectra, the emission characteristics of the PVA/GA–chitosan blend films change with the GA–chitosan concentration (Fig. 6(a)). With increasing the GA–chitosan concentration from 4 to 8% in the PVA blends, a new emission band emerges in the cyan region of the electromagnetic spectrum (485 nm). The intensity of the emission band increases with increasing the GA–chitosan concentration. The occurrence of this shoulder peak in the emission curves may suggest that the new luminescence contribution comes from excimer-type arrangements in the solid state (Halkyard, Rampey, Kloppenburg, Studer-Martinez, & Bunz, 1998). Actually, this phenomenon, caused by the presence of dimers with associated excited electronic states, is favored by the π–π stacking interactions among the GA–chitosan molecules, and is probably promoted by the more planar chromophore conformation in the solid state (Bunz, 2000; Pucci, Bertoldo, & Bronco, 2005). Based on the 8% GA–chitosan–PVA blend, the fluorescence emission bands are entirely red-shifted and the emission intensity is markedly increased after the incorporation of silica nanoparticles. The intensity is also increased with increasing the nano-silica loading, as displayed in the fluorescence emission curves in Fig. 6(b). When excited at 280 nm, an emission feature characterized by a well-defined vibronic structure is attributed to the 0–0, 0–1, and 0–2 radiative transitions, appearing at 426, 476, and 526 nm, respectively. Moreover, the UV–vis absorption spectra of silica nanocomposite films show broader and stronger bands than those of the blend films without inorganic components. These results indicate that the silica nanoparticles have a positive impact on both the fluorescence emission of fluorophore and UV absorption with respect to GA–chitosan. It is well known that the larger the isolation extent of fluorophores, the stronger the fluorescence and higher photostability can be. Nano-silica acts as a protective coating on individual fluorophore, preventing the GA–chitosan from aggregation and leading to a highly effective isolation of the GA–chitosan

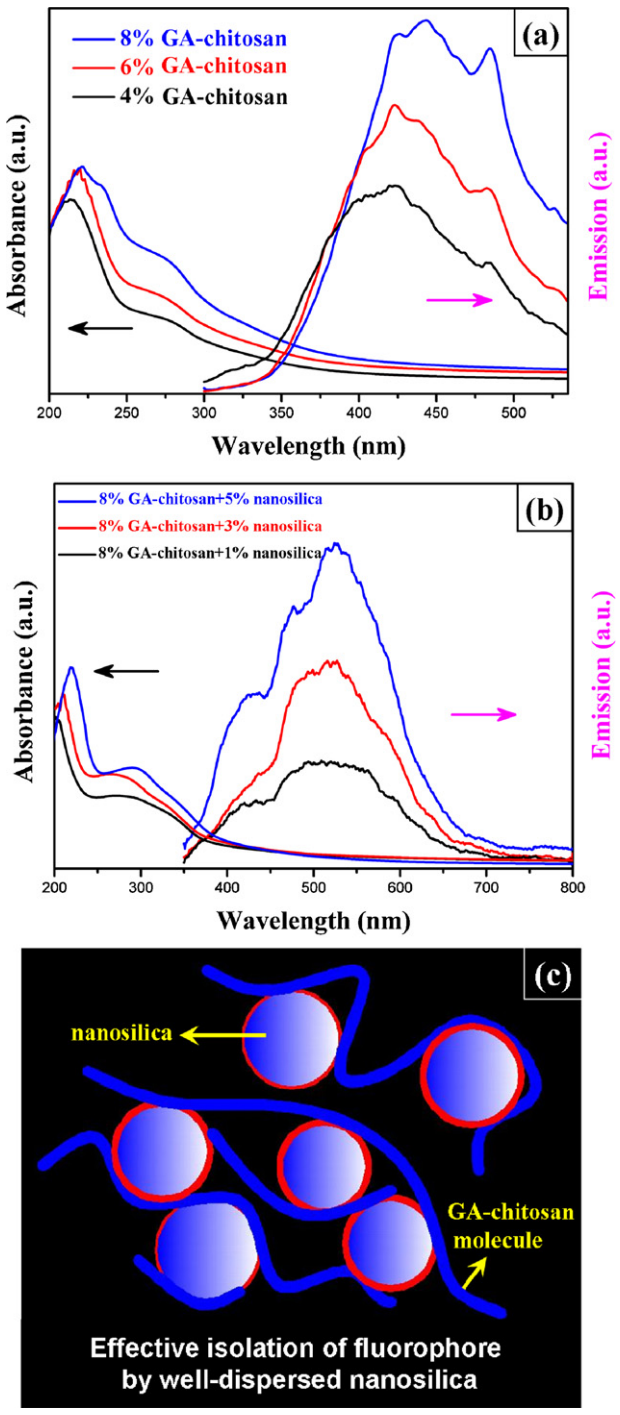

Fig. 6. UV–vis absorption and fluorescence emission spectra (λ_{exc} = 280 nm) of the PVA/GA–chitosan blend films as a function of GA–chitosan concentration (a), and 8% GA–chitosan–PVA blend based nanocomposite films with 1, 3, and 5% nano-silica loadings (b); schematic illustration (c) of the silica reinforcement of fluorescence by effective isolation of fluorophore.

molecules. Fig. 6(c) shows the schematic diagram of the effective isolation of fluorophore by the well-dispersed nano-silica. Furthermore, stiff silica nanoparticles having strong interactions with GA–chitosan molecules will increase the stiffness of the fluorescent conjugated planar structure, resulting in an enhanced fluorescent efficiency.

TGA was used to characterize the thermal properties of the GA–chitosan, pure PVA, and PVA based blend and nanocomposite films whose TG curves are shown in Fig. 7. With respect to

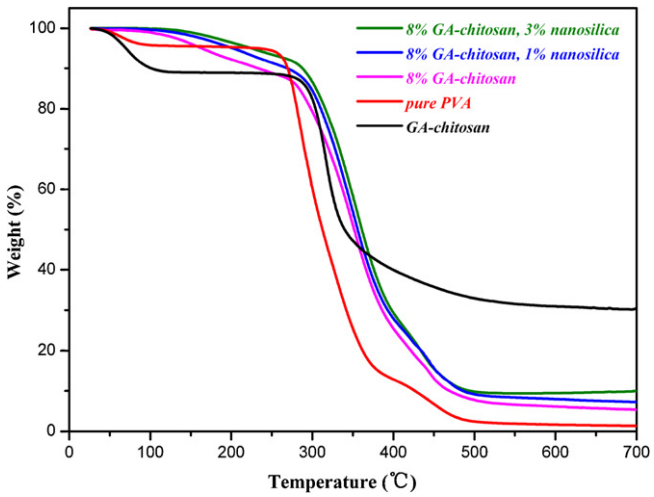

Fig. 7. TG patterns of the GA–chitosan, pure PVA, and PVA based blend and nanocomposite materials.

the neat GA–chitosan, the water content calculated is about 11.0%, which indicates that the GA–chitosan contains one water molecule per polymeric unit (Neto et al., 2005). As for the pure PVA sample, the content of surface-adsorbed water is about 4.4%, which implicates that the pure PVA is sensitive to water. When compounded with 8% GA–chitosan, its water resistance is improved. Nevertheless, the thermal stability of the blend is similar to that of the pure PVA in the temperature range below about 275 °C. With the incorporation of the inorganic nano-silica, the thermal stabilities of the GA–chitosan–PVA based nanocomposites are improved in the whole temperature range. The increase of about 30 °C of decomposition temperature is obtained for the 8% GA–chitosan–PVA blend based nanocomposites filled with 3% nano-silica, as compared with that of the pure PVA.

Scanning electron micrographs of the GA–chitosan, nano-silica, and PVA based composites with GA–chitosan and nano-silica are displayed in Fig. 8. As shown in Fig. 8(a) and (b), a sheet-like structure can be observed for the GA–chitosan. Various sizes of GA–chitosan can be found in the images, and the cross-linked chitosan is believed to form the large bulk sheets, together with the remaining undisturbed chitosan (with a much smaller size) dispersed around the GA–chitosan. As for the nano-silica, several individual nanoparticles are combined into a cluster, with an average diameter of about 60 nm, which is about 5 times bigger than that of the isolated particle (with a diameter of 5–15 nm), as shown in Fig. 8(c) and (d). The small clusters attach to each other, and form a big aggregate. This result means that the individual nanoparticles have the strong interactions with each other due to the hydrogen bonding effect through the silanol groups. The freeze-fractured section of the 8% GA–chitosan–PVA blend is shown in Fig. 8(e) and (f), in which the molecular homogeneous dispersion of GA–chitosan in the PVA matrix can be observed, which confirms the absence of microsized aggregates of the luminescent molecules, and the presence of highly effective fluorescence. Therefore, the GA–chitosan is well dispersed in the amorphous phase of the polymer matrix down to the SEM resolution. When the nano-silica was incorporated into the 8% GA–chitosan–PVA blend, the crystal structure was changed. As presented in Fig. 8(g)–(l), with increasing the loading of SiO_2 nanoparticles, the nanoparticles embedded in polymer matrix and protruded from the freeze-fractured surface can be more clearly observed, with a larger number of displayed particles (the loadings of the nano-silica from 1% to 3%, and to 5% are shown in Fig. 8(g) and (h), (i) and (j), and (k) and (l), respectively). These results indicate that the nano-inclusions have disturbed the molecular interactions

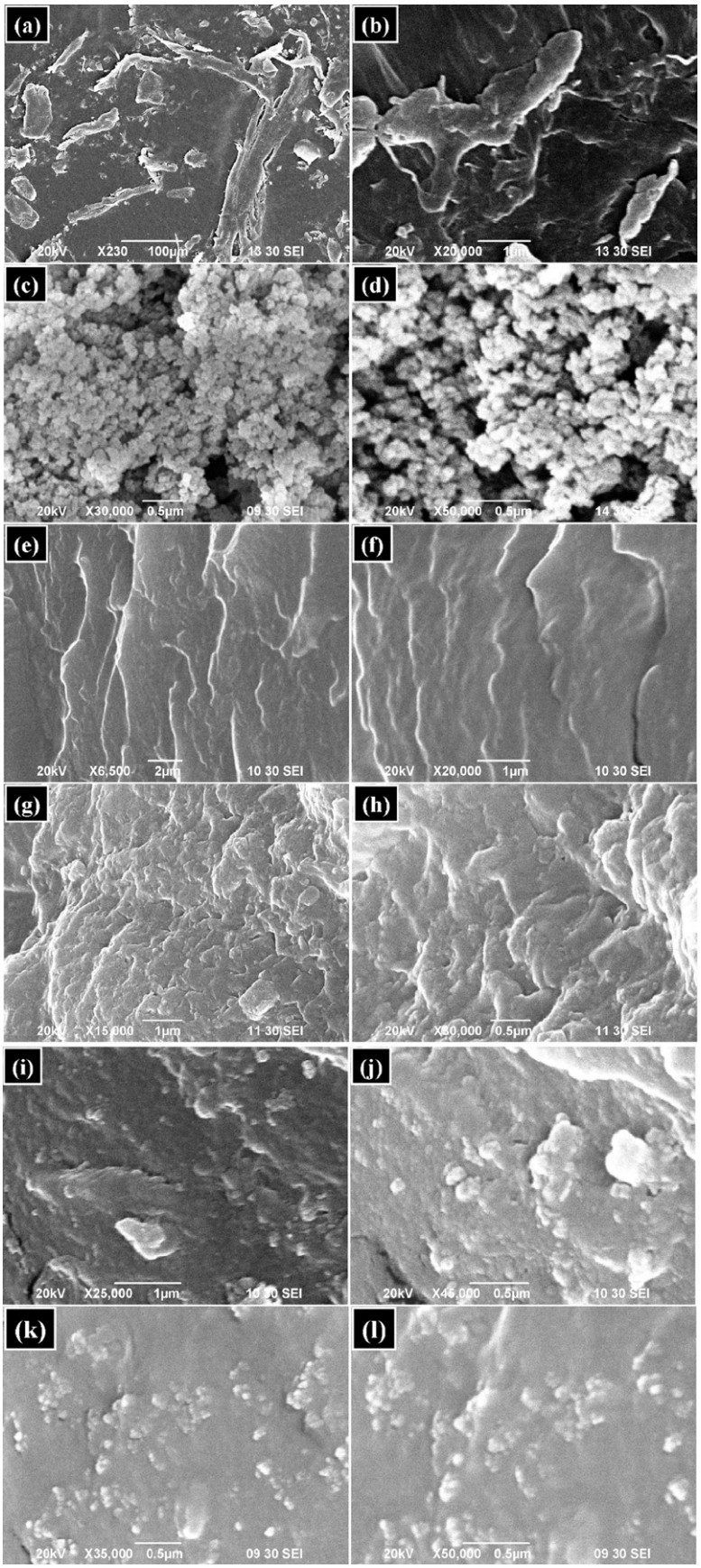

Fig. 8. SEM images of the GA–chitosan (a and b), neat nano-silica (c and d), freeze-fractured sections of 8% GA–chitosan–PVA blend film (e and f), 8% GA–chitosan–PVA blend based nanocomposite film with 1% (g and h), 3% (i and j), and 5% nano-silica (k and l). The right image was captured at a high resolution-scale from the left one.

in the polymer blend system, resulting in the decrease of polymer crystallinity, as discussed in XRD and DSC sections. With increasing the loading of nano-silica, the morphology of the nanocomposites gradually turns to be amorphous. When the loading reaches 5%, an almost complete amorphous block decorated with numerous silica nanoparticles can be observed.

4. Conclusions

In this work, the autofluorescent GA–chitosan was blended with a poly (vinyl alcohol) matrix to generate the transparent and fluorescent blend films. The fluorescent efficiency is increased with increasing the concentration of the GA–chitosan, with the red-shifted fluorescent emission band, and the formation of a new emission band located in the wavelength region which corresponds to the cyan color image. Moreover, the introduction of the GA–chitosan into the PVA matrix considerably decreases the polymer crystallinity. The incorporation of the silica nanoparticles into the GA–chitosan–PVA blend further increases the fluorescent efficiency, along with the red-shifted emission band to a longer wavelength, in addition to the further reduction of PVA crystallinity. Therefore, these fluorescence properties can be finely tuned by changing the polymer crystallinity and doping of the polymer matrix with the silica nanoparticles. In addition, the water and heat resistances of the GA–chitosan–PVA based silica nanocomposites can be markedly enhanced as compared with the GA–chitosan–PVA two-component system. It is expected that the developed biodegradable polymer based blends and nanocomposites, with both the transparent and fluorescent properties, can pave a way for the fluorescent probe, drug-carrier, and tracer applications.

Acknowledgments

This work was financially supported by a grant from the Innovation and Technology Commission of The Government of the Hong Kong Special Administrative Region, China, in the form of an ITF project (Project No. GHP/063/09TP). We thank Mr. Jianghua Lee and Dr. Sherry Bao (The Hong Kong polytechnic University) for their assistance for the fluorescence characterization and valuable advices.

References

Bandi, S., & Schiraldi, D. A. (2006). Glass transition behavior of clay aerogel/poly (vinyl alcohol) composites. *Macromolecules*, *39*(19), 6537–6545.

Bruni, G., Gozzo, F., Capsoni, D., Bini, M., Macchi, P., Simoncic, P., et al. (2011). Thermal, spectroscopic, and ab initio structural characterization of carprofen polymorphs. *Journal of Pharmaceutical Sciences*, *100*(6), 2321–2332.

Bunz, U. (2000). Poly(aryleneethynylene)s: Syntheses, properties, structures, and applications. *Chemical Reviews*, *100*(4), 1605–1644.

Chandy, T., & Sharma, C. P. (1992). Prostaglandin E1-immobilized poly(vinyl alcohol)-blended chitosan membranes: Blood compatibility and permeability properties. *Journal of Applied Polymer Science*, *44*(12), 2145–2156.

Chen, H., Wang, F., Zhang, C., Shi, Y., Jin, G., & Yuan, S. (2010). Preparation of nano-silica materials: The concept from wheat straw. *Journal of Non-Crystalline Solids*, *356*(50), 2781–2785.

Cho, H. J., Jung, B. J., Cho, N. S., Lee, J., & Shim, H. K. (2003). Synthesis and characterization of thermally stable blue light-emitting polyfluorenes containing siloxane bridges. *Macromolecules*, *36*(18), 6704–6710.

Chuang, W. Y., Young, T. H., Yao, C. H., & Chiu, W. Y. (1999). Properties of the poly (vinyl alcohol)/chitosan blend and its effect on the culture of fibroblast in vitro. *Biomaterials*, *20*(16), 1479–1487.

Depla, A., Lesthaeghe, D., van Erp, T. S., Aerts, A., Houthoofd, K., Fan, F., et al. (2011). 29Si NMR and UV-Raman investigation of initial oligomerization reaction pathways in acid-catalyzed silica sol–gel chemistry. *The Journal of Physical Chemistry C*, *115*(9), 3562–3571.

Goldsmith, P. C., & Brezina, L. R. (1982). Gnrh neuronal systems in the basal hypothalamus of the neonatal baboon. *Journal of Histochemistry and Cytochemistry*, *30*(6), 574.

Halkyard, C. E., Rampey, M. E., Kloppenburg, L., Studer-Martinez, S. L., & Bunz, U. H. F. (1998). Evidence of aggregate formation for 2,5-dialkylpoly (p-phenyleneethynylenes) in solution and thin films. *Macromolecules*, *31*(25), 8655–8659.

Hiromi, N., Tomoaki, Y., Akihiro, A., Tokuyuki, Y., Saeko, T., Toshiro, H., et al. (2011). Effect of surface properties of silica nanoparticles on their cytotoxicity and cellular distribution in murine macrophages. *Nanoscale Research Letters*, *6*.

Jin, J., Smith, D. W., Jr., Topping, C. M., Suresh, S., Chen, S., Foulger, S. H., et al. (2003). Synthesis and characterization of phenylphosphine oxide containing perfluorocyclobutyl aromatic ether polymers for potential space applications. *Macromolecules*, *36*(24), 9000–9004.

Jongsomjit, B., Chaichana, E., & Praserthdam, P. (2005). LLDPE/nano-silica composites synthesized via in situ polymerization of ethylene/1-hexene with MAO/metallocene catalyst. *Journal of Materials Science*, *40*(8), 2043–2045.

Koyano, T., Koshizaki, N., Umehara, H., Nagura, M., & Minoura, N. (2000). Surface states of PVA/chitosan blended hydrogels. *Polymer*, *41*(12), 4461–4465.

Minoura, N., Koyano, T., Koshizaki, N., Umehara, H., Nagura, M., & Kobayashi, K. (1998). Preparation, properties, and cell attachment/growth behavior of PVA/chitosan-blended hydrogels. *Materials Science and Engineering C*, *6*(4), 275–280.

Monton, M. R. N., Forsberg, E. M., & Brennan, J. D. (2012). Tailoring sol–gel-derived silica materials for optical biosensing. *Chemistry of Materials*, *24*(5), 796–811.

Muzzarelli, R. A. A. (1977). *Chitin*. Oxford, UK: Pergamon Press.

Nakatsuka, S., & Andrady, A. L. (1992). Permeability of vitamin B-12 in chitosan membranes. Effect of crosslinking and blending with poly(vinyl alcohol) on permeability. *Journal of Applied Polymer Science*, *44*(1), 17–28.

Neto, C. G. T., Giacometti, J., Job, A., Ferreira, F., Fonseca, J., & Pereira, M. (2005). Thermal analysis of chitosan based networks. *Carbohydrate Polymers*, *62*(2), 97–103.

Ohno, K., Shimoaka, T., Akai, N., & Katsumoto, Y. (2008). Relationship between the broad OH stretching band of methanol and hydrogen-bonding patterns in the liquid phase. *The Journal of Physical Chemistry A*, *112*(32), 7342–7348.

Ow, H., Larson, D. R., Srivastava, M., Baird, B. A., Webb, W. W., & Wiesner, U. (2005). Bright and stable core–shell fluorescent silica nanoparticles. *Nano Letters*, *5*(1), 113–117.

Peng, Z., & Kong, L. X. (2007). A thermal degradation mechanism of polyvinyl alcohol/silica nanocomposites. *Polymer Degradation and Stability*, *92*(6), 1061–1071.

Peng, Z., Kong, L. X., Li, S. D., & Spiridonov, P. (2006). Poly (vinyl alcohol)/silica nanocomposites: Morphology and thermal degradation kinetics. *Journal of Nanoscience and Nanotechnology*, *6*(12), 3934–3938.

Pucci, A., Bertoldo, M., & Bronco, S. (2005). Luminescent bis (benzoxazolyl) stilbene as a molecular probe for poly (propylene) film deformation. *Macromolecular Rapid Communications*, *26*(13), 1043–1048.

Qi, L., Xu, Z., Jiang, X., Hu, C., & Zou, X. (2004). Preparation and antibacterial activity of chitosan nanoparticles. *Carbohydrate Research*, *339*(16), 2693–2700.

Ravi Kumar, M. N. V., Muzzarelli, R. A. A., Muzzarelli, C., Sashiwa, H., & Domb, A. J. (2004). Chitosan chemistry and pharmaceutical perspectives. *Chemical Reviews*, *104*, 6017–6084.

Srinivasa, P., Ramesh, M., Kumar, K., & Tharanathan, R. (2003). Properties and sorption studies of chitosan–polyvinyl alcohol blend films. *Carbohydrate Polymers*, *53*(4), 431–438.

Verraedt, E., Pendela, M., Adams, E., Hoogmartens, J., & Martens, J. (2010). Controlled release of chlorhexidine from amorphous microporous silica. *Journal of Controlled Release*, *142*(1), 47–52.

Wang, T., Turhan, M., & Gunasekaran, S. (2004). Selected properties of pH-sensitive, biodegradable chitosan–poly(vinyl alcohol) hydrogel. *Polymer International*, *53*(7), 911–918.

Wei, W., Wang, L. Y., Yuan, L., Wei, Q., Yang, X. D., Su, Z. G., et al. (2007). Preparation and application of novel microspheres possessing autofluorescent properties. *Advanced Functional Materials*, *17*(16), 3153–3158.

Xia, R., Heliotis, G., Campoy-Quiles, M., Stavrinou, P., Bradley, D., Vak, D., et al. (2005). Characterization of a high-thermal-stability spiroanthracenefluorene-based blue-light-emitting polymer optical gain medium. *Journal of Applied Physics*, *98*, 083101.

Yang, C. Q., Lu, Y., & Lickfield, G. C. (2002). Chemical analysis of 1,2,3,4-butanetetracarboxylic acid. *Textile Research Journal*, *72*(9), 817–824.

Yang, J. M., Su, W. Y., Leu, T. L., & Yang, M. C. (2004). Evaluation of chitosan/PVA blended hydrogel membranes. *Journal of Membrane Science*, *236*(1), 39–51.

Yoon, J., Lee, H. J., & Stafford, C. M. (2011). Thermoplastic elastomers based on ionic liquid and poly (vinyl alcohol). *Macromolecules*, *44*(7), 2170–2178.

Yu, Q., Song, Y., Shi, X., Xu, C., & Bin, Y. (2011). Preparation and properties of chitosan derivative/poly (vinyl alcohol) blend film crosslinked with glutaraldehyde. *Carbohydrate Polymers*, *84*(1), 465–470.